Integration of High Reliability Distribution System in Microgrid Operation

Mohammad E. Khodayar, *Member, IEEE*, Masoud Barati, and Mohammad Shahidehpour, *Fellow, IEEE*

***Abstract*—In this paper, the application of high reliability distribution system (HRDS) in the economic operation of a microgrid is studied. HRDS, which offers higher operation reliability and fewer outages in microgrids, is applied to looped networks in distribution systems. The microgrid model in this study is composed of distributed energy resources (DER) including distributed generation (DG), controllable loads, and storage. The microgrid would utilize the local DER as well as the main grid for supplying its hourly load economically which is subject to power quality and reliability requirements. The HRDS implemented at Illinois Institute of Technology (IIT) is used as a case study along with the local DER to increase the load point reliability and decrease the operation cost of the IIT microgrid. The availability of distribution lines, main grid supply, and microgrid generation is considered using the Markov chain Monte Carlo simulation in the microgrid scenarios. The reliability indices based on frequency and duration of outages are measured at the microgrid level and the load point level, and the potential system enhancements are discussed for improving the economic operation of the IIT microgrid.**

***Index Terms*—High reliability distribution system, microgrid economics, stochastic security constrained unit commitment, storage.**

NOMENCLATURE

Variables

$E^{(\cdot)}_{k,t}$	Available energy in storage unit k at time t.
$F_{c,(\cdot)}$	Production cost function of a DG unit.
g	Denote the main grid connection.
i	Denote a DG unit.
k	Denote a storage unit.
$I^{(\cdot)}_{(\cdot)}$	Unit status; 1 means on and 0 means off.
$I^{(\cdot)}_{c,(\cdot)}$	Indicator of storage unit in charging mode.
$I^{(\cdot)}_{dc,(\cdot)}$	Indicator of storage unit in discharging mode.
j, o	Index of bus.
$P^{(\cdot)}_{(\cdot)}$	Dispatch of a unit/grid generation.
$P^{(\cdot)}_{c,(\cdot)}, P^{(\cdot)}_{dc,(\cdot)}$	Charge/discharge power of storage unit.
$P^{d,(\cdot)}_{j,(\cdot)}, Q^{d,(\cdot)}_{j,(\cdot)}$	Real/reactive served load at bus j.
$P^{inj,(\cdot)}_{j,(\cdot)}, Q^{inj,(\cdot)}_{j,(\cdot)}$	Real/reactive injection at bus j.
$PL^{(\cdot)}_{j,o}$	Real power flow between buses j and o.
$Q^{(\cdot)}_{(\cdot)}$	Reactive power generation of a unit.
$QL^{(\cdot)}_{j,o}$	Reactive power flow between buses j and o.
s	Denote a scenario.
$SD^{(\cdot)}_{(\cdot)}$	Shutdown cost of a generation unit.
$SL^{(\cdot)}_{j,o}$	Apparent power flow between buses j and o.
$SU^{(\cdot)}_{(\cdot)}$	Startup cost of a generation unit.
t	Hour index.
$V^{s}_{j,t}$	Voltage of bus j at hour t in scenario s.
$\theta^{(\cdot)}_{(\cdot)}$	Bus voltage angle.

Constants

$B^{(\cdot)}_{(\cdot)}$	Imaginary part of microgrid admittance matrix.
$b^{(\cdot)}_{j,o}$	Susceptance of the branch between buses j and o.
CS_i, CD_i	Startup/shutdown cost of the thermal DG unit i.
$D^{(\cdot)}_{j}$	Set of units/loads which are connected to bus j.
$E^{\min}_{k}, E^{\max}_{k}$	Min/max energy stored in storage unit k.
$G^{(\cdot)}_{(\cdot)}$	Real part of microgrid admittance matrix.
$g^{(\cdot)}_{j,o}$	Conductance of the branch between buses j and o.
NB	Total number of buses in the system.
NT	Total number of hours under study.
p^s	Probability of scenario s.
$P^{\min}_{(\cdot)}, P^{\max}_{(\cdot)}$	Min/max generation capacity.
$P^{\min}_{c,k}, P^{\max}_{c,k}$	Min/max charging capacity of storage unit k.

Manuscript received May 04, 2012; revised June 29, 2012; accepted July 23, 2012. Date of publication September 28, 2012; date of current version December 28, 2012. This work was supported in part by the U.S. Department of Energy under Grant DE-FC26-08NT02875. Paper no. TSG-00250-2012.

The authors are with Electrical and Computer Engineering Department, Illinois Institute of Technology, Chicago, IL 60616 USA (e-mail: mkhodaya@iit.edu; mbarati@iit.edu; ms@iit.edu).

Color versions of one or more of the figures in this paper are available online at http://ieeexplore.ieee.org.

Digital Object Identifier 10.1109/TSG.2012.2213348

$P_{dc,k}^{\min}, P_{dc,k}^{\max}$	Min/max discharging capacity of storage unit k.
$P_{D,t}$	Total microgrid load.
$P_{j,(.)}^{D}$	Load at bus j.
$Q_{(.)}^{\min}, Q_{(.)}^{\max}$	Min/max reactive power capacity of unit.
$r_{j,o}, x_{j,o}$	Line resistance & reactance between buses j and o.
$SL_{o,j}^{\max}$	Maximum line capacity between buses j and o.
$U_{j,o}^{(\cdot)}$	Line availability between buses j and o.
$UX_{(\cdot)}^{(\cdot)}$	Generation availability, 1 if available, otherwise 0.
$VOLL$	Value of lost load.
$y_{j,o}$	Admittance connected between buses j and o.
ρ_t	Hourly price of the grid supply.
η_k	Charge/discharge cycle efficiency of storage unit k.

I. Introduction

MICROGRIDS are considered as viable options for the electrification in university campuses, military installations, and other locations where the main grid expansion is either impossible or has no economic justification [1]. The operation and control of microgrids with distributed energy resources (DER) could also reduce the transmission burden on a power utility system. DER in a microgrid could include combined heat and power (CHP), photovoltaic (PV), small wind turbines (WT), heat or electricity storage, and controllable loads. DER applications increase the efficiency of energy supply and reduce the electricity delivery cost and carbon footprint in a microgrid. DER applications could also make it possible to impose intentional islanding in microgrids [2]. The proximity of generation to loads in microgrids could improve the power quality and reliability (PQR) at load points.

The emergence of microgrids in power utility systems has raised additional technical, economical, and regulatory challenges [3]. Matching generation and load to maintain the frequency and managing reactive power to regulate voltages and minimize losses are important issues in microgrid operations especially when microgrids are operated in an island mode. Storage devices including batteries, super-capacitors, and flywheels are used to match generation with load in microgrids. Storage can supply generation deficiencies, reduce load surges by providing ride-through capability for short periods [4], reduce network losses [5], and improve the protection system by contributing to fault currents [6].

The operation and control of automated switches can improve PQR indices in microgrids. Proper control signals would ensure the economics and the security of microgrids in grid-connected and island modes. Control schemes in microgrids include hierarchical and decentralized controls. The decentralized control facilitates distributed control and management of large complex systems by offering small autonomous systems referred to as agents. However, decentralized control requires significant experimentation with coordination before implementation and could introduce security challenges [7]. In [8], the economic operation of microgrids is evaluated by incorporating a hierarchical control. Hierarchical control is performed by a master controller which matches generation and load for real and reactive power control. The voltage-reactive power and frequency-real power characteristics of DGs would provide the required real and reactive power to adjust the voltage and frequency in microgrids. The master controller is responsible for maintaining the frequency in a microgrid by adjusting DG according to their frequency droop characteristics, utilizing storage, and load shedding. Moreover, voltage control strategies can be utilized by the master controller considering the voltage/reactive power droop of DGs so that there would be no reactive circulating currents among such resources. The Kyotango microgrid project in Japan is an example of hierarchically controlled microgrid [1]. In [9]–[11], the role of power sharing is evaluated to regulate the frequency and the voltage in microgrids.

From the reliability point of view, microgrids can provide higher reliability and power quality at load points. The proximity of DG and load could decrease the duration and the frequency of outages as well as the level of energy not supplied at a microgrid [12], [13]; however, the microgrid topology could play a crucial role in supplying the microgrid loads with diverse reliability requirements. In a grid-connected mode, outages of the main grid could lead to the microgrid islanding. In the island mode, the master controller relies on the microgrid generation and storage to balance the load with generation and prevent load curtailments. The load-supply balancing in an islanded microgrid could depend on the load priority and reliability requirements. In [14], the effect of load-supply mismatch on the microgrid reliability indices is evaluated by incorporating the stochastic nature of DGs. Reference [15] addresses the load serving sequence in microgrids considering load point reliability indices.

This paper will evaluate the effect of HRDS switches and storage facilities on increasing the reliability indices in looped distribution systems. HRDS is introduced and applied to the IIT microgrid and the improvements on reliability indices are evaluated. The proposed reliability indices include the system average interruption frequency index (SAIFI), system average interruption duration index (SAIDI), customer average interruption duration index (CAIDI), customer average interruption frequency index (CAIFI), expected energy not supplied (EENS), and loss of load expectation (LOLE). The numerical results show that the integration of HRDS switches will help improve the reliability indices in a microgrid. Moreover, it is shown that integrating storage will not only improve the reliability indices in a microgrid but also reduce the operation cost at consumer levels. Section II introduces the HRDS and automatic switches. Section III presents the mathematical formulation and the solution methodology for the optimal operation and control of microgrids. Section IV presents an overview of the IIT microgrid and Section V discusses the optimal operation and control of IIT microgrid and evaluates the effect of HRDS on the IIT microgrid and consumer reliability indices. The conclusions are presented in Section VI.

II. High Reliability Distribution System

The implementation of microgrid loops is made possible by the use of automatic switches in HRDS. An example of HRDS is to apply Vista switches, equipped with SF_6 gas insulated

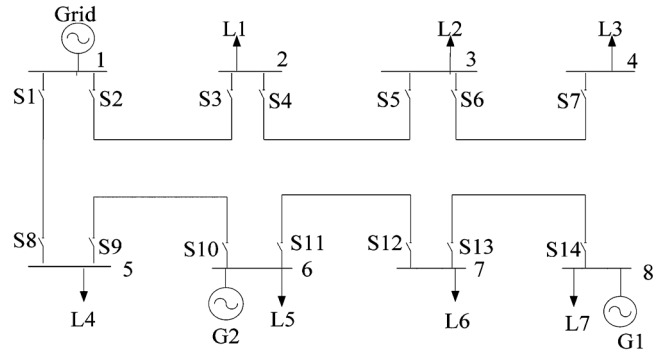

Fig. 1. Sample of a microgrid without HRDS switches.

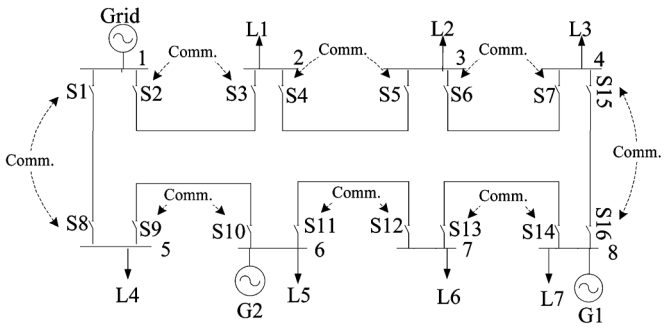

Fig. 2. Sample of a microgrid with HRDS switches.

fault interrupters, manufactured by the S&C Electric Company. HRDS switches can sense the cable faults and isolate the faulted section with no impact on other sections in a microgrid. The master controller will monitor the status of each HRDS switch using the supervisory control and data acquisition (SCADA) system. The master controller is responsible for economic operation of the microgrid based on signals received from switches on the status of distribution branches. Fig. 1 shows the sample microgrid network with a traditional protection scheme. Fig. 2 shows the HRDS implementation.

Comparing Figs. 1 and 2, it is clear that any line outages in microgrid shown in Fig. 1 will lead to load interruptions. In Fig. 1, if a fault occurs on the line connecting buses 2 and 3, the switches 4 and 5 will open and the load at buses 3 and 4 will be interrupted. In Fig. 2, if a fault occurs on the line connecting buses 2 and 3, switches 4 and 5 detect the fault according to the fault current direction and clear the fault without any interruptions to the loads at buses 3 and 4. Hence, loads will remain in service. In this case, all switches remain closed except S4 and S5. By incorporating the fiber optic technology for the communications between switches and fast response directional relays, the fault in Fig. 2 is cleared in less than 6 cycles (0.1 sec) which will not be sensed by the other microgrid loads.

The relays incorporated in HRDS switchgears provide permissive over-reaching transfer trip (POTT) and directional comparison blocking (DCB) protection. Before isolation, POTT monitors the direction of over-current relays on both sides of the cable to confirm that there is a fault. DCB acts as a backup protection system which tends to isolate the fault once the short circuit current is sensed by switches; however, POTT sends blocking signals if a fault is not occurred between the switches. As a backup protection scheme, DCB is always active in the microgrid even if the distribution system is open-looped. Fiber optics is used as a communication medium between relays and switches. The fiber optic communication system is capable of transferring the information in less than 2 msec which enables the main protection system to clear the fault in less than 6 cycles. The backup non-directional over current protection will operate if the primary protection scheme or the communication system fails.

III. Optimal Operation of Microgrids

At steady state, the microgrid master controller will minimize the operation cost of DG, including startup and shutdown costs, the cost of energy supplied by the main grid, and penalty costs (i.e., value of lost load) associated with the microgrid load curtailments. The optimal solution is subject to microgrid and the main grid constraints. The master controller will create an islanded microgrid in the case of grid contingencies and supply the microgrid loads by the local microgrid generation.

In this paper, a stochastic security-constrained unit commitment formulation is proposed for the master controller which is solved using the mixed-integer programming (MIP) model for the microgrid generation, grid supply and battery storage. The master controller objective and constraints are shown in (1)–(25). The load balance constraint is shown in (2). The mismatch represents the lost load, which is minimized in the objective function by penalizing the value of lost load. Equations (3) and (4) represent the startup and shutdown costs of local generation. The real and reactive power generation constraints by the local and the main grid generation are shown in (5)–(8), respectively. The substation transformers/breakers will limit the energy trades with the main grid. Microgrid outages could further constrain such trades.

The microgrid storage will store energy when the market price of electricity is low and supply energy to the microgrid when the hourly market price is high. The storage constraints are shown in (9)–(16). The dispatch of storage unit is represented by (9). The constraint on the storage commitment is represented by (10) and charge/discharge capacity limits are shown in (11), (12). The reactive power supplied by power electronic interface of the storage unit is shown in (13) [20]. The available energy at hour t is shown in (14) which is dependent on the available energy at hour $(t-1)$ and the charged/discharged energy at hour t. In (14), the hourly charged/discharged energy is restricted by the charge/discharge cycle efficiency of the storage unit. The limitation on stored energy which is represented by min/max state of charge of the storage unit is represented by (15) and (16). The net injected real/reactive power at each bus is shown in (17), (18). Equation (19) shows the admittance of distribution lines. The linearized formulation of real/reactive power injections are given in (20), (21). Equations (22) and (23) show the linearized formulation of real and reactive line flow and (24) represents the apparent power flow through the distribution line. Here, $\zeta_{j,o}^{t,s}$ is an auxiliary parameter, which is dependent on the load power factor as calculated in Appendix. The constraint on apparent power flow which is enforced by the line capacity is shown in (25).

Random outages are considered in the main grid and the microgrid. The Monte Carlo representation of outages is applied and the Latin Hypercube Sampling (LHS) technique is used to develop a large number of scenarios with equal probabilities. A two-state Markov chain process is utilized to represent microgrid outages according to the microgrid component outage and repair rates. The scenario reduction technique is applied to reduce the number of generated scenarios to an acceptable level with the corresponding probabilities. Scenario reduction will eliminate the low probability scenarios and bundle scenarios that are close in terms of statistical metrics [16]–[18].

The MIP formulation in each scenario is decomposed into a master problem and several subproblems based on the linear programming duality theory [21]. In each scenario, the master problem determines the hourly unit commitment and dispatch solution of generation and storage facilities while the subproblems will check the distribution network constraints. In the case of violations, Benders cuts are generated and added to the master problem. The master problem is solved with the new constraints and the network constraints are checked in the next step. This iterative process will continue until there is no further transmission violation [21]–[23].

$$Min \sum_s p^s \left(\sum_t \sum_i \left(F^s_{c,i}\left(P^s_{i,t}\right) + SU^s_{i,t} + SD^s_{i,t} \right) + \rho_t \cdot P^s_{g,t} + VOLL. \left(\sum_t \sum_j P^D_{j,t} - P^{d,s}_{j,t} \right) \right) \quad (1)$$

s.t.

$$\sum_i P^s_{i,t} + P^s_{g,t} + \sum_k P^s_{k,t} = \sum_j P^{d,s}_{j,t} \quad (2)$$

$$SU^s_{i,t} \geq CS_i \cdot \left(I^s_{i,t} - I^s_{i,t-1} \right) \quad (3)$$

$$SD^s_{i,t} \geq CD_i \cdot \left(I^s_{i,t-1} - I^s_{i,t} \right) \quad (4)$$

$$P^{\min}_i \cdot UX^s_{i,t} \cdot I^s_{i,t} \leq P^s_{i,t} \leq P^{\max}_i \cdot UX^s_{i,t} \cdot I^s_{i,t} \quad (5)$$

$$P^{\min}_g \cdot UX^s_{g,t} \leq P^s_{g,t} \leq P^{\max}_g \cdot UX^s_{g,t} \quad (6)$$

$$Q^{\min}_i \cdot I^s_{i,t} \cdot UX^s_{i,t} \leq Q^s_{i,t} \leq Q^{\max}_i \cdot I^s_{i,t} \cdot UX^s_{i,t} \quad (7)$$

$$Q^{\min}_g \cdot UX^s_{g,t} \leq Q^s_{g,t} \leq Q^{\max}_g \cdot UX^s_{g,t} \quad (8)$$

$$P^s_{k,t} = P^s_{dc,k,t} - P^s_{c,k,t} \quad (9)$$

$$I^s_{dc,k,t} + I^s_{c,k,t} \leq 1 \quad (10)$$

$$I^s_{c,k,t} \cdot P^{\min}_{c,k} \leq P^s_{c,k,t} \leq I^s_{c,k,t} \cdot P^{\max}_{c,k} \quad (11)$$

$$I^s_{dc,k,t} \cdot P^{\min}_{dc,k} \leq P^s_{dc,k,t} \leq I^s_{dc,k,t} \cdot P^{\max}_{dc,k} \quad (12)$$

$$Q^{\min}_k \cdot \left(I^s_{dc,k,t} + I^s_{c,k,t} \right) \leq Q^s_{k,t} \leq Q^{\max}_k \cdot \left(I^s_{dc,k,t} + I^s_{c,k,t} \right) \quad (13)$$

$$E^s_{k,t} = E^s_{k,t-1} - \left(P^s_{dc,k,t} - \eta_k \cdot P^s_{c,k,t} \right) \quad (14)$$

$$E^{\min}_k \leq E^s_{k,t} \leq E^{\max}_k \quad (15)$$

$$E_{k,0} = E_{k,NT} \quad (16)$$

$$\sum_{i \in D^i_j} P^s_{i,t} + \sum_{g \in D^g_j} P^s_{g,t} + \sum_{k \in D^k_j} P^s_{k,t} - \sum_{d \in D^d_j} P^{d,s}_{D,t} = P^{inj,s}_{j,t} \quad (17)$$

$$\sum_{i \in D^i_j} Q^s_{i,t} + \sum_{g \in D^g_j} Q^s_{g,t} + \sum_{k \in D^k_j} Q^s_{k,t} - \sum_{d \in D^d_j} Q^{d,s}_{D,t} = Q^{inj,s}_{j,t} \quad (18)$$

$$y^{t,s}_{o,j} = g^{t,s}_{o,j} + Jb^{t,s}_{o,j} = \frac{r_{o,j} \cdot U^{t,s}_{o,j}}{r^2_{o,j} + x^2_{o,j}} - J \frac{x_{o,j} \cdot U^{t,s}_{o,j}}{r^2_{o,j} + x^2_{o,j}} \quad (19)$$

$$P^{inj,s}_{j,t} = \left(2V^s_{j,t} - 1 \right) \cdot G^{t,s}_{j,j} + \sum_{o(j \neq o)}^{NB} G^{t,s}_{j,o} \left(V^s_{j,t} + V^s_{o,t} - 1 \right) + B^{t,s}_{j,o} \left(\theta^s_{j,t} - \theta^s_{o,t} \right) \quad (20)$$

$$Q^{inj,s}_{j,t} = -\left(2V^s_{j,t} - 1 \right) \cdot B^{t,s}_{j,j} + \sum_{o(j \neq o)}^{NB} - B^{t,s}_{j,o} \left(V^s_{j,t} + V^s_{o,t} - 1 \right) + G^{t,s}_{j,o} \left(\theta^s_{j,t} - \theta^s_{o,t} \right) \quad (21)$$

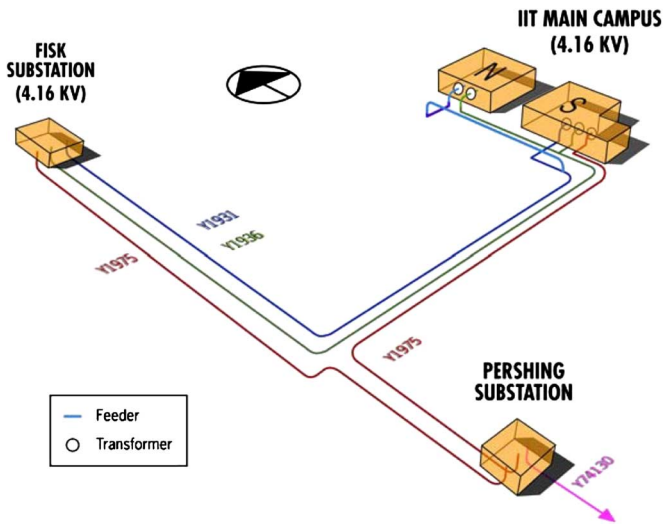

Fig. 3. ComEd system configuration feeding IIT substations [24].

$$PL^{t,s}_{j,o} = G^{t,s}_{j,o} \left(V^{t,s}_j - V^{t,s}_o \right) + B^{t,s}_{j,o} \left(\theta^{t,s}_j - \theta^{t,s}_o \right) \quad (22)$$

$$QL^{t,s}_{j,o} = B^{t,s}_{j,o} \left(V^{t,s}_o - V^{t,s}_j \right) + G^{t,s}_{j,o} \left(\theta^{t,s}_j - \theta^{t,s}_o \right) \quad (23)$$

$$SL^{t,s}_{j,o} = PL^{t,s}_{j,o} + \xi^{t,s}_{j,o} \cdot QL^{t,s}_{j,o} \quad (24)$$

$$\left| SL^{t,s}_{j,o} \right| \leq SL^{\max}_{j,o} \quad (25)$$

IV. The Perfect Power System—IIT Microgrid

In 2004–2006, the underground distribution system at IIT suffered 12 unplanned power outages which disrupted academic and administrative activities and damaged several pieces of operation and research equipment. The outages were due to partial or complete loss of the utility supply and malfunctions of aged cables and other distribution components at IIT. The lack of system redundancy and the unavailability of replacement components prolonged the outage durations at IIT. In 2005, the Galvin Electricity Initiative led a campaign to implement a perfect power system at IIT with the objective of establishing a microgrid that is environmentally friendly, fuel efficient, robust, and resilient with a self-healing capability. The microgrid at IIT empowers the campus consumers, in response to the real time price of electricity, to control daily power consumptions. IIT microgrid enhances its operation reliability by applying a real-time reconfiguration of power distribution assets, real-time islanding of critical loads, and real-time optimization of power supply resources.

Fig. 3 shows the configuration of the ComEd distribution network (main grid) that feeds the IIT microgrid. IIT is supplied by three 12.47 KV circuits fed from the ComEd Fisk substation. The peak load at IIT is approximately 10 MW. The IIT's 4.16 KV distribution system consists of 12.47/4.16 kV transformers, supply/feeder breakers and building transformers. Siegel Hall is the pilot building for the perfect power demonstration which is fed through the primary—which is backed up by a secondary (redundant)—feeder equipped with automatic switch. The voltage is further stepped down to 120 V in the building.

In Fig. 4, the IIT microgrid consists of seven loops. The North Substation feeds three loops while the South Substation supplies energy to the remaining loops. Each building is supplied by redundant feeders which are normally energized to ensure that the building is fed by an alternate path in the case of an outage.

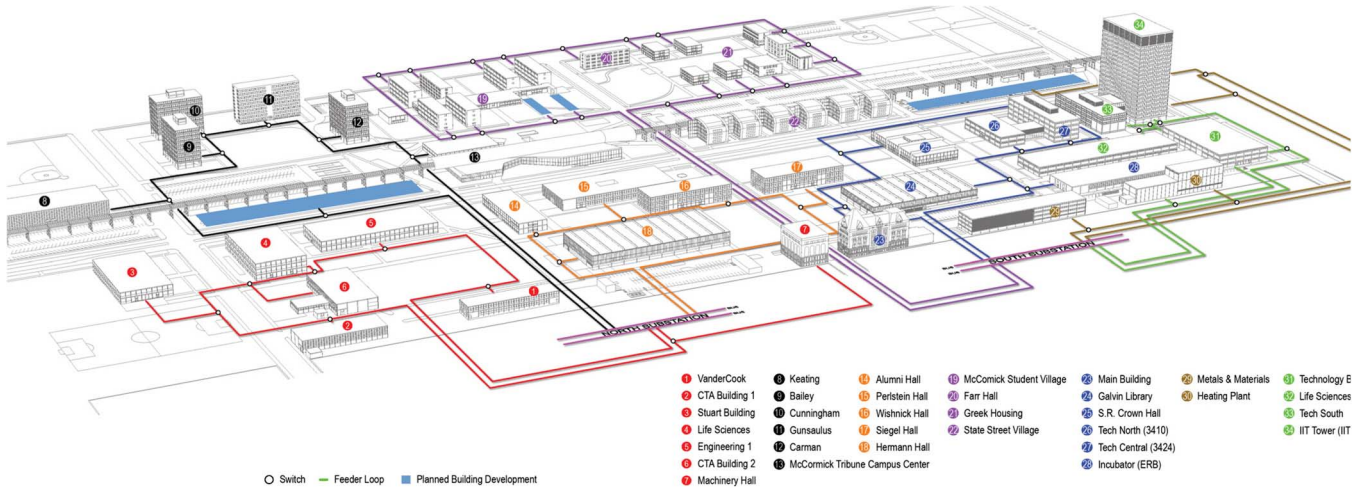

Fig. 4. IIT distribution system layout based on HRDS.

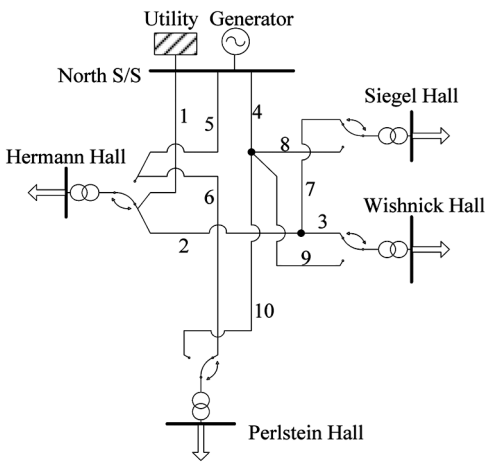

Fig. 5. Third loop layout without HRDS switches.

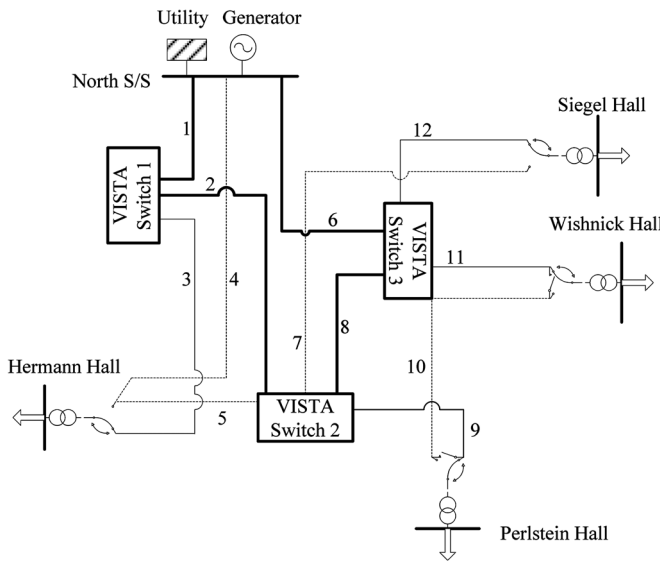

Fig. 6. Third loop layout with HRDS switches.

The HRDS at IIT utilizes Vista underground closed loop fault-clearing switchgear with SEL-351 directional over-current protection relays. The fault isolation takes place in a quarter of a cycle by automatic breakers. The communication system is via fiber optic cables which facilitate the coordination between switches.

In Fig. 4, the third loop which is connected to the North Substation consists of five buildings including Hermann Hall, Wishnick Hall, Siegel Hall, Perlstein Hall, and Alumni Hall. Figs. 5 and 6 show the third loop with and without HRDS switches. It is also assumed that the redundant cables in Figs. 5 and 6 will be available when the primary feeding cable has failed. The load at Perlstein and Alumni Hall are aggregated as the Perlstein Hall load. In Fig. 5, an outage will result in downstream load curtailments until the manual switching restores the loads. Since the transfer switches are manually operated, the estimated time for manual source transfer at the building feeder is about 3 h. In Fig. 6, the HRDS switches at load points provide uninterruptable load serving capability. Here, buildings are referred to as customers throughout the paper.

The IIT microgrid generation includes combustion microturbines connected to the North Substation as well as renewable energy sources. The IIT microgrid is equipped with an 8 MW gas-fired power plant which includes two 4 MW Rolls Royce gas turbines. The microgrid generation could be used for reliability and economic improvements in the main grid-connected and the island modes.

Renewable energy sources include wind and solar generation. An 8 kW Viryd wind turbine is installed on the north side of the campus in the Stuart soccer field. 60 kW of PV cells are installed on two building rooftops to supply portions of campus load. A 500 kWh ZBB storage is installed on campus to increase the reliability and efficiency of the IIT microgrid. Moreover, several electric vehicle charging stations are deployed on campus to utilize the microgrid energy storage and provide green energy for on campus electric vehicles.

A major element of the IIT microgrid is its master controller. Master controller applies a hierarchical control via SCADA to ensure reliable and economic operation of the IIT microgrid. It also coordinates the operation of HRDS controllers, on-site generation, storage, and individual building controllers [25]. Intelligent switching and advanced coordination technologies of master controller through communication systems facilitates rapid fault assessments and isolations in the IIT microgrid [24]. Fig. 7 shows the overview of the control tasks performed by master controller at IIT.

The IIT microgrid participates in real-time electricity markets. Once the real-time price exceeds 7–8 cents per kWh (mar-

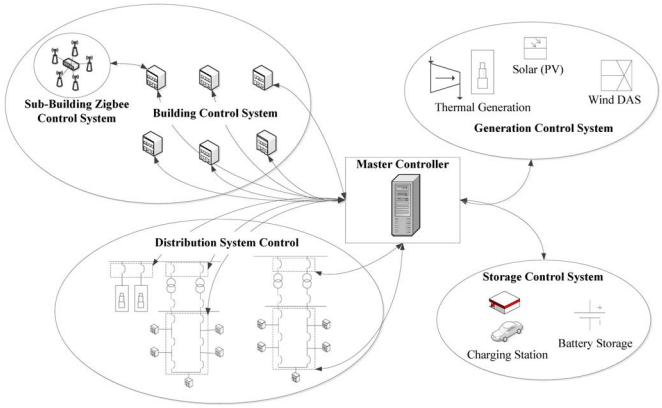

Fig. 7. Overview of the master controller system.

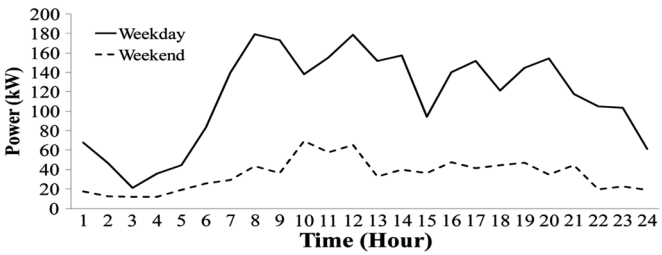

Fig. 8. Load pattern in Hermann hall.

ginal cost of microgrid generation), the microgrid generation could serve the IIT load. The on-site generation can provide demand response and increase the reliability. The provision of spinning reserve and day ahead load response is also offered by master controller by managing microgrid generation, storage, controllable loads, power quality devices, and smart switches.

V. Simulation of IIT Microgrid Operation

The master controller simulation at steady state and in contingencies (with and without HRDS) is considered. The simulation period is one year. The maximum loads at Hermann, Siegel, Wishnick, and Perlstein Halls are 289 kW, 167 kW, 272 kW, and 513 kW, respectively. The typical Hermann Hall load is shown in Fig. 8, in which the weekend load is approximately 30% of that of weekdays.

Tables I and II show the IIT distribution system characteristics with and without HRDS respectively. The line numbers are shown in Figs. 5 and 6. It is assumed that the backup lines are always available once they are energized to serve the loads. For example, in Fig. 5, once Lines 1, 2, or 3 fail, the Wishnick Hall load is served through Lines 4 and 9. Here, the microgrid generation capacity is 1 MW. The mean time to failure (MTTF) for the microgrid generation and grid supply is 1200 h and the mean time to repair (MTTR) of microgrid generation and grid supply is 25 h. For simplicity, the charge/discharge efficiency and the availability of storage and HRDS switches are assumed to be 100%. The maximum charge/discharge rate of the 500 kWh ZBB storage unit is 250 kW/h.

The stochastic solution of microgrid provides the expected economic and reliability indices once HRDS switches and storage are integrated into the IIT microgrid. The availability of distribution lines, grid supply, and microgrid generation is considered in scenarios using the Markov chain Monte Carlo (MCMC) simulation. The Monte Carlo simulation is

TABLE I
Cable Characteristic at IIT Microgrid With HRDS

Line ID	Resistance (Ω/1000 ft)	Inductance (Ω/1000 ft)	Length (ft.)	Failure Rate (/yr)	MTTR (hr)	MTTF (hr)
1	0.028	0.037	159.2	0.2866	20	30,565
2	0.028	0.037	435.9	0.7846	20	11,164
3	0.028	0.037	144.5	0.2601	20	33,679
4	0.028	0.037	261.3	-	-	-
5	0.028	0.037	584	-	-	-
6	0.028	0.037	1,409.9	2.5378	20	3,451
7	0.028	0.037	755.7	-	-	-
8	0.028	0.037	452.7	0.8148	20	10,751
9	0.028	0.037	65.7	0.1182	20	74,111
10	0.028	0.037	376.8	-	-	-
11	0.028	0.037	99.4	0.1789	20	48,965
12	0.028	0.037	76.0	0.1368	20	64,035

TABLE II
Cable Characteristic at IIT Microgrid Without HRDS

Line ID	Resistance (Ω/1000 ft)	Inductance (Ω/1000 ft)	Length (ft.)	Failure Rate (/yr)	MTTR (hr)	MTTF (hr)
1	0.028	0.037	145.8	0.2624	20	33,384
2	0.028	0.037	382.6	0.6886	20	12,721
3	0.028	0.037	100.5	0.1809	20	48,424
4	0.028	0.037	758.1	-	-	-
5	0.028	0.037	182.6	0.3286	20	26,658
6	0.028	0.037	407.9	0.7342	20	11,931
7	0.028	0.037	250.0	0.45	20	19,466
8	0.028	0.037	238.5	-	-	-
9	0.028	0.037	92.6	-	-	-
10	0.028	0.037	30	-	-	-

applied to generate a large number of scenarios. The scenario reduction is applied to select 10 scenarios corresponding to Figs. 5 and 6 with their assigned probabilities. The reliability indices of microgrid are calculated and compared with and without HRDS switches. In the following, the contribution of master controller, HRDS, and storage to the reliability and the optimality of microgrid are evaluated for the eighth scenario, followed by a discussion on the results in other scenarios.

In the following, two options for the modeling of campus microgrid are studied. Option A applies a deterministic operation by considering the eighth scenario as the only alternative for the microgrid operation, and option B analyzes the stochastic behavior of the IIT microgrid.

A. Deterministic Operation of Microgrid

In this case, one scenario is closely analyzed and the effect of HRDS and the storage system on the microgrid reliability indices is evaluated. The following cases are studied:

Case 1) IIT microgrid is not equipped with HRDS switches (Fig. 5).

Case 2) IIT microgrid is equipped with HRDS switches (Fig. 6).

Case 3) IIT microgrid is equipped with HRDS switches and the storage system which is located next to Hermann Hall.

TABLE III
IIT MICROGRID WITH HRDS (START AND END DATE OF OUTAGE, day/hr)

	Grid	Power Plant	L1	L2	L6	L8
First Outage	2/6-2/8	88/19-88/21	212/12-212/18	7/6-8/16	67/17-69/1	59/20
Second Outage	5/1-7/6	146/11-147/7	-	-	174/14-175/12	-
Third Outage	38/10-39/21	334/13-336/23	-	-	-	-
Fourth Outage	193/9-194/10	337/20-338/17	-	-	-	-
Fifth Outage	201/18-202/9	343/22-345/1	-	-	-	-
Sixth Outage	280/12-280/19	-	-	-	-	-
Seventh Outage	284/13-289/17	-	-	-	-	-
Eighth Outage	311/18-311/23	-	-	-	-	-

Table III shows the annual incidents with HRDS in the eighth scenario. The table shows that the first grid outage took place in the second day at hour 6 with two-hour duration while the second outage occurred on the fifth day which required a two-day repair. In the eighth scenario, there are five cable outages in the system equipped with HRDS switches while there is only one cable outage in the system without HRDS switches. Without HRDS, line L6 failed on the 224th day at hour 23 and was restored on the 225th day at hour 6. The outages of the main grid and DG are the same in both systems. In this scenario, we could have additional outages with HRDS because there are more components in a loop; however, the loads have never been interrupted.

1) Economic Operation of Microgrid: The microgrid operation cost includes the cost of main grid energy transactions (in both directions), cost of microgrid energy supply, and curtailment costs (value of lost load.) The operation cost of storage is assumed negligible. When the hourly market price of energy is higher than the marginal cost of microgrid generation, the microgrid could supply its excess energy to the main grid for reducing its operation cost. The main grid electricity prices in this study are based on historical hourly electricity prices of commercial customers [26].

Proper protective devices are located in the microgrid at the point of common coupling (PCC) which enables bi-directional power flows. The failure rate of the grid indicates the failure rate of the interface facilities at PCC. It is assumed that the price of electricity for trading with the grid is the same as the grid LMP at PCC.

The microgrid outages could result in the loss of revenue estimated at 80 $/kWh (value of lost load) which covers the replacement cost of the damaged equipment (campus facilities as well as those in laboratories), personnel and administrative cost of restoring and sustaining research and educational experiments, cost of aggravation associated with disrupted academic classes, laboratories, and any other major campus events such as open houses and conferences that are interrupted by microgrid outages.

The annual operation cost in Case 1 is 140 497 $/yr. The HRDS implementation reduces the operation cost to 126 644 $/yr. The use of storage will further reduce the annual operation cost to 119 236 $/yr by performing demand response and taking daily market price fluctuations into account. The lost loads in the three Cases are 173.236, 0, and 0 kWh/yr, respectively.

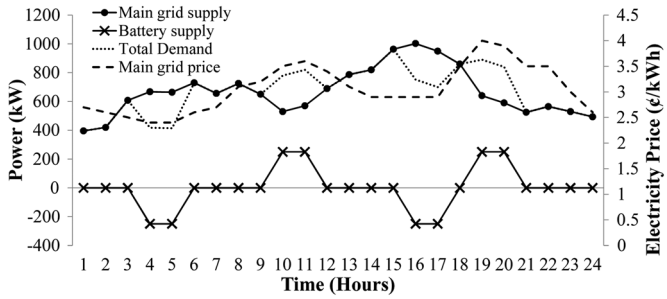

Fig. 9. Storage and the main grid supply on the 23rd day.

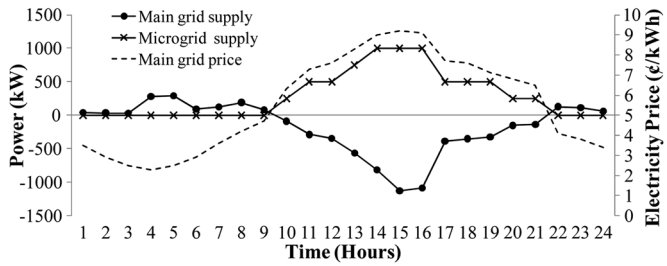

Fig. 10. Microgrid and the main grid supply on the 217th day.

Fig. 9 shows the microgrid energy flow on the 23rd day of the year. Here the energy drawn from the main grid is stored at the storage when the main grid hourly prices are low (hours 4, 5, 16, and 17) and deployed once the main grid prices are high (hours 10, 11, 19, and 20.) The main grid prices in Fig. 9 are not high enough to trigger the local microgrid generation. The lowest prices at the microgrid occurs at hours 4 and 5 (2.4 ¢/kWh) which increase to 3.5 and 3.6 ¢/kWh at hours 10 and 11, respectively. This cycle is repeated at hours 16–17 and 19–20.

Fig. 10 shows the energy supply to the microgrid on the 217th day (summer day) when the main grid electricity prices are higher. Here, the local microgrid generation is dispatched at hour 10 when the main grid prices are higher than 6 ¢/kWh. The microgrid revenue for a single day energy sale is $473.699.

2) Microgrid Reliability Evaluation: In this case, interruption indices for consumers and the entire microgrid are evaluated. There are four customers in the third loop. In Case 1, there is a single load interruption in Perlstein Hall, so SAIFI and CAIFI are 0.25 (interruption/customer.yr) and 1 (interruption/affected customer.yr) respectively. The outage duration is 3 h and SAIDI and CAIDI are 0.75 (hrs/customer.yr) and 3 (hrs/customer interruption.yr) respectively. In Case 2, no microgrid outages occur which decreases SAIFI, CAIFI, SAIDI, and CAIDI to zero. Likewise, in Case 3, SAIFI, CAIFI, SAIDI, and CAIDI are zero.

The results show that the HRDS integration will decrease the microgrid outage duration and frequency in Case 2, and lower the microgrid SAIFI, SAIDI, CAIDI, and CAIFI. In Cases 2 and 3, we could have additional outages with HRDS because there are more components in a loop; however, the loads would never be interrupted as shown in Table IV. In the eighth scenario, there is only one outage at L6 in Case 1 which lasts 9 h. Since the manual switching takes 3 h and the building is fed by the redundant path after manual switching, this event leads to a 3 hour outage and 173.236 kWh energy not supplied in Perlstein Hall. The EENS and LOLE in this case are 173.236 kWh/yr and 3 h/yr respectively. In Cases 2 and 3 there are 5 cable outages

TABLE IV
ANNUAL ENERGY NOT SUPPLIED AT LOAD POINTS

	Hermann Hall (kWh/yr)	Siegel Hall (kWh/yr)	Wishnick Hall (kWh/yr)	Perlstein Hall (kWh/yr)
Case1	0	0	0	173.236
Case 2	0	0	0	0
Case 3	0	0	0	0

TABLE V
PROBABILITY OF STOCHASTIC SCENARIOS AFTER SCENARIO REDUCTION

Scenario No.	1	2	3	4	5
Probability	0.107	0.119	0.126	0.0326	0.084
Scenario No.	6	7	8	9	10
Probability	0.125	0.092	0.108	0.0964	0.11

TABLE VI
OPERATION COST OF STOCHASTIC SCENARIOS IN CASE 1

Scenario No.	1	2	3	4	5
Operation Cost ($/yr)	182,655	191,727	154,340	730,330	232,863
Scenario No.	6	7	8	9	10
Operation Cost ($/yr)	226,398	192,773	140,497	238,694	303,518

TABLE VII
OPERATION COST OF STOCHASTIC SCENARIOS IN CASE 2

Scenario No.	1	2	3	4	5
Operation Cost ($/yr)	127,087	125,041	125,750	609,400	124,609
Scenario No.	6	7	8	9	10
Operation Cost ($/yr)	127,544	127,861	126,644	152,777	146,649

TABLE VIII
OPERATION COST OF SCENARIOS IN CASE 3

Scenario No.	1	2	3	4	5
Operation Cost ($/yr)	119,525	117,513	118,223	549,537	117,108
Scenario No.	6	7	8	9	10
Operation Cost ($/yr)	120,045	119,109	119,236	122,157	120,968

which lasted 103 h; however, these events did not interrupt the served loads because of HRDS.

B. Stochastic Solution of Microgrid Operation

1) Operation Cost: A scenario reduction technique was applied to select 10 scenarios from a large number of scenarios generated by the MCMC method [27], [28]. The scenario reduction algorithms include fast backward, fast forward/backward and fast backward/backward methods [28]. The algorithms are chosen according to the size of the stochastic problem and the required solution accuracy. For large scenario trees, the fast forward method provides a more accurate solution with a longer processing time. In this paper, a fast backward/forward method is used for the scenario reduction. The probabilities of 10 stochastic scenarios are shown in Table V.

The operation costs of scenarios are shown in Tables VI–VIII. Here, the operation cost of Case 2 is lower than that in Case 1 in all scenarios because HRDS can reduce the energy not supplied and its respective penalties. The storage will also reduce the duration of microgrid load curtailments and the annual energy not supplied. Comparing Tables VIII and VII, it is shown that the cost in Case 3 is decreased as compared to that in Case 2. The expected operation costs in Cases 1–3 are 224 073 $/yr, 146 899 $/yr, and 120 038 $/yr respectively. The estimated saving at the IIT microgrid with HRDS installed at all seven loops is 621 867 $/yr.

TABLE IX
MICROGRID AND CONSUMER INTERRUPTION INDICES IN CASE 1

Scenario No.	1	2	3	4	5
SAIFI (int./cust.yr)	0.25	1.25	0.5	3.5	1.5
SAIDI (hr/ cust. yr)	0.75	2.25	1.5	18	3.75
CAIFI (int./aff. cust. yr)	1	1.25	1	3.5	3
CAIDI (hr/cust. int. yr)	3	1.8	3	5.14	2.5
Scenario No.	6	7	8	9	10
SAIFI (int./cust.yr)	1.25	0.75	0.25	2.5	2.25
SAIDI (hr/ cust. yr)	3.75	1.75	0.75	5.25	5.75
CAIFI (int./aff. cust. yr)	1.66	1	1	3.33	2.25
CAIDI (hr/cust. int. yr)	3	2.33	3	2.1	2.55

TABLE X
MICROGRID AND CONSUMER INTERRUPTION INDICES IN CASE 2

Scenario No.	1	2	3	4	5
SAIFI (int./cust.yr)	0	0	0	1.75	0
SAIDI (hr/ cust. yr)	0	0	0	12.75	0
CAIFI (int./aff. cust. yr)	0	0	0	1.75	0
CAIDI (hr/cust. int. yr)	0	0	0	7.28	0
Scenario No.	6	7	8	9	10
SAIFI (int./cust.yr)	0	0.25	0	0.75	0.25
SAIDI (hr/ cust. yr)	0	0.25	0	1	0.5
CAIFI (int./aff. cust. yr)	0	1	0	1	1
CAIDI (hr/cust. int. yr)	0	1	0	1.33	2

TABLE XI
MICROGRID AND CONSUMER INTERRUPTION INDICES IN CASE 3

Scenario No.	1	2	3	4	5
SAIFI (int./cust.yr)	0	0	0	1.25	0
SAIDI (hr/ cust. yr)	0	0	0	11.25	0
CAIFI (int./aff. cust. yr)	0	0	0	1.25	0
CAIDI (hr/cust. int. yr)	0	0	0	9	0
Scenario No.	6	7	8	9	10
SAIFI (int./cust.yr)	0	0	0	0	0
SAIDI (hr/ cust. yr)	0	0	0	0	0
CAIFI (int./aff. cust. yr)	0	0	0	0	0
CAIDI (hr/cust. int. yr)	0	0	0	0	0

2) Microgrid Reliability indices: Tables IX–XI show the microgrid system and customer interruption indices in stochastic scenarios. Table X shows the HRDS reduces SAIFI and SAIDI; however, it may not decrease CAIDI and CAIFI consistently. In the seventh scenario, CAIFI is not reduced in Case 2 because fewer outages will affect fewer customers proportionally which leads to an equal frequency of interruption per affected customer per year. In Case 1, there are 3 outages which affect 3 customers. In Case 2, there is a single outage which affected one customer; hence the CAIFI in Cases 1 and 2 are equal. In the fourth scenario, CAIDI in Case 2 is increased as compared to Case 1. The reason for a higher CAIDI is that the frequency of interruption drops faster than the duration of interruption; hence the duration of interruption per affected customer per year is higher.

In Case 2, the duration of interruption is 51 h/yr and the frequency of interruptions is 7, while in Case 1, the duration of interruption is 72 h and the frequency of interruption is 14. Although the frequency of interruption is decreased by a half, the duration of interruption is not decreased proportionally, leaving a higher CAIDI in Case 2. In Case 2, most scenarios have lower CAIDI and CAIFI than those in Case 1. Although it is not shown, CAIFI can also be higher in some scenarios in Case 2, as compared to that in Case 1, if the number of outages and the affected customers are not reduced proportionally.

TABLE XII
ENERGY NOT SUPPLIED AT LOAD POINTS IN CASE 1 (kWh/yr)

Scenario No.	1	2	3	4	5
Hermann Hall	0	56.662	0	1,413.705	0
Wishnick Hall	0	495.024	0	1,951.124	0
Siegel Hall	0	32.803	292.129	1,370.819	404.838
Perlstein Hall	694.830	249.597	65.467	2,802.999	948.843
Total	694.830	834.086	357.596	7,538.647	1,353.681
Scenario No.	6	7	8	9	10
Hermann Hall	172.573	0	0	0	437.242
Wishnick Hall	658.611	17.793	0	622.114	1,129.902
Siegel Hall	405.045	84.496	0	645.066	580.567
Perlstein Hall	0	903.08	173.236	96.612	42.08
Total	1,236.229	1,005.369	173.236	1,363.792	2,189.791

TABLE XIII
ENERGY NOT SUPPLIED AT LOAD POINTS IN CASE 2 (kWh/yr)

Scenario No.	1	2	3	4	5
Hermann Hall	0	0	0	1,451.496	0
Wishnick Hall	0	0	0	1,356.101	0
Siegel Hall	0	0	0	791.003	0
Perlstein Hall	0	0	0	2,427.678	0
Total	0	0	0	6,026.278	0
Scenario No.	6	7	8	9	10
Hermann Hall	0	17.793	0	61.401	227.972
Wishnick Hall	0	0	0	68.201	0
Siegel Hall	0	0	0	159.771	0
Perlstein Hall	0	0	0	0	0
Total	0	17.793	0	289.373	227.972

CAIDI is dependent on the duration and the frequency of outages. In some scenarios, CAIDI is higher because the frequency and the duration of outages are not reduced proportionally. So the HRDS implementation will lead to shorter frequency and duration for outages with lower SAIFI and SAIDI.

In Case 3, SAIFI, SAIDI and CAIFI are reduced as compared to that in Case 2; however, CAIDI in the fourth scenario is higher. In this scenario, there are 7 outages in Case 2 as compared to 5 outages in Case 3, and the outage duration is dropped from 51 h in Case 2 to 45 h in Case 3. Hence, CAIDI is higher in Case 3 since the duration of interruption drops more slowly than its frequency.

In Table XII, scenario 4 corresponds to a generation failure when the grid fails. In this case, the storage unit would supply the load partially which is supplemented by the microgrid load curtailment. Table V shows a lower probability in this case.

Although interruption frequency indices are lower, the integration of microgrid storage may not decrease SAIFI and CAIFI in all scenarios since the storage will lower the unserved load rather than the frequency of interruptions. However, the expected SAIFI and CAIFI will be lower when the storage is implemented. When the storage is introduced, SAIFI, SAIDI, CAIFI, and CAIDI are lowered to zero in Scenarios 7, 9, and 10, which shows that the storage can eliminate the energy not supplied. In summary, SAIDI and SAIFI are lowered in all scenarios once the HRDS is installed and SAIDI is lower with the microgrid storage in place.

Table XVI shows lower expected SAIFI, SAIDI, CAIFI, and CAIDI when HRDS is implemented and demonstrates an enhance reliability when the storage is used. Tables XII–XIV show the energy not supplied. As expected, Case 3 shows the lower energy not supplied in each scenario due to storage. HRDS will lead to lower energy not supplied with the lowest expected energy not supplied in Case 3 followed by that of Case 2.

Storage can also reduce the LOLE in microgrids. In Table XV, Case 3 demonstrates the lowest outage hours followed by that in Case 2. The LOLE in Cases 1–3 are 13.15, 2.36, and 1.47 hr/yr which are reduced with HRDS switches and storage. Here, microgrid load shedding occurs when the main grid supply is unavailable. Table XVI shows the enhancements in Cases 2 and 3.

TABLE XIV
ENERGY NOT SUPPLIED AT LOAD POINTS IN CASE 3 (kWh/yr)

Scenario No.	1	2	3	4	5
Hermann Hall	0	0	0	1,248.662	0
Wishnick Hall	0	0	0	1,017.405	0
Siegel Hall	0	0	0	769.404	0
Perlstein Hall	0	0	0	2,335.710	0
Total	0	0	0	5,371.181	0
Scenario No.	6	7	8	9	10
Hermann Hall	0	0	0	0	0
Wishnick Hall	0	0	0	0	0
Siegel Hall	0	0	0	0	0
Perlstein Hall	0	0	0	0	0
Total	0	0	0	0	0

TABLE XV
TOTAL OUTAGE DURATION IN CASES AND SCENARIOS (hr/yr)

Scenario No.	1	2	3	4	5
Case 1	3	9	6	72	15
Case 2	0	0	0	51	0
Case 3	0	0	0	45	0
Scenario No.	6	7	8	9	10
Case 1	15	7	3	21	23
Case 2	0	1	0	4	2
Case 3	0	0	0	0	0

TABLE XVI
EXPECTED RELIABILITY AND ECONOMIC INDICES

Case	1	2	3
Exp. SAIFI (int./cust.yr)	1.22	0.18	0.04
Exp. SAIDI (hr/ cust. yr)	3.29	0.59	0.37
Exp. CAIFI (int./aff. cust. yr)	1.73	0.36	0.04
Exp. CAIDI (hr/cust. int. yr)	2.69	0.68	0.29
Exp. Operation Cost ($/yr)	224,073	146,899	120,038
Exp. Energy not Supplied (kWh/yr)	1,216.21	251.07	175.10
LOLE (hr/yr)	13.153	2.360	1.467

VI. CONCLUSIONS

In this paper, reliability and economic indices of a microgrid equipped with HRDS switches is analyzed. The simulation of the IIT microgrid is presented and the contributions are highlighted as follows:

- The stochastic AC network formulation for the master controller is offered to solve the hourly unit commitment and economic dispatch in microgrids.
- The role of local generation, main grid, and energy storage on the economic operation of microgrids is considered and the enhanced reliability indices at load points are calculated.
- Storage can reduce the operation cost of a microgrid by performing demand response and avoiding emergency load curtailments. Storage helps mitigate the expected interruption duration and frequency and improves the customer reliability in microgrids.
- HRDS is used for the evaluation of reliability and economic indices in microgrids which are compared to those in traditional distribution systems.

- The implementation of HRDS and automatic switches can reduce the expected frequency and the duration of interruptions and the expected energy not supplied in microgrids. HRDS can also reduce the expected operation cost of a microgrid by mitigating emergency load curtailments and reducing the value of lost loads.
- Microgrid reliability indices are calculated with/without HRDS.
- It is estimated that the expected operation cost at the IIT microgrid would be lowered by $621 867 annually by integrating HRDS; the storage can further reduce the operation cost by $109 220.

APPENDIX

$\zeta_{j,o}^{t,s}$, derived here, is an auxiliary parameter which is dependent on the load power factor. The apparent power flow through the line is written as

$$SL_{j,o}^{t,s} = \sqrt{\left(PL_{j,o}^{t,s}\right)^2 + \left(QL_{j,o}^{t,s}\right)^2} \tag{A1}$$

$$SL_{j,o}^{t,s} = PL_{j,o}^{t,s} \cdot \sqrt{1 + \left(\frac{QL_{j,o}^{t,s}}{PL_{j,o}^{t,s}}\right)^2} \tag{A2}$$

Using Taylor series

$$SL_{j,o}^{t,s} = PL_{j,o}^{t,s} \cdot \left(1 + \frac{1}{2} \cdot \left(\frac{QL_{j,o}^{t,s}}{PL_{j,o}^{t,s}}\right)^2\right) \tag{A3}$$

$$SL_{j,o}^{t,s} = PL_{j,o}^{t,s} + \frac{1}{2} \cdot QL_{j,o}^{t,s} \cdot \tan\theta_{j,o}^{t,s} \tag{A4}$$

where

$$\xi_{j,o}^{t,s} = \frac{1}{2} \cdot \tan\theta_{j,o}^{t,s} \tag{A5}$$

$$\theta_{j,o}^{t,s} = \tan^{-1}\left(\frac{Q_j^{t,s} + Q_o^{t,s}}{P_j^{t,s} + P_o^{t,s}}\right) \tag{A6}$$

REFERENCES

[1] G. Venkataramanan and C. Marnay, "A larger role for microgrids," *IEEE Power and Energy Mag.*, vol. 6, no. 3, May 2008.

[2] N. Hatziargyriou, H. Asano, M. R. Iravani, and C. Marnay, "Microgrids: An overview of ongoing research, development and demonstration projects," *IEEE Power and Energy Mag.*, vol. 5, no. 4, Jul./Aug. 2007.

[3] B. Kroposki, R. Lasseter, T. Ise, S. Morozumi, S. Papathanassiou, and N. Hatziargyriou, "Making microgrids work," *IEEE Power and Energy Mag.*, vol. 6, no. 3, May 2008.

[4] J. Kim, J. Jeon, S. Kim, C. Cho, J. H. Park, H. Kim, and K. Nam, "Cooperative control strategy of energy storage system and microsources for stabilizing the microgrid during islanded operation," *IEEE Trans. Power Electronics*, vol. 25, no. 12, Sep. 2010.

[5] U. Kwhannet, N. Sinsuphun, U. Leeton, and T. Kulworawanichpong, "Impact of energy storage in microgrid systems with DGs," in *Proc. International conference on power system technology (POWERCON)*, Hangzhou, Oct. 2010.

[6] N. Jayawarna, C. Jones, M. Barnes, and N. Jenkins, "Operating microgrid energy storage control during network faults," in *IEEE International Conference on Systems Engineering*, San Antonio, Texas, Apr. 2007.

[7] K. E. Nygard *et al.*, "Decision support independence in a smart grid," in *Proc. Second International Conference on Smart Grids, Green Communications and IT Energy-aware Technologies*, Mar. 2012, pp. 69–74.

[8] A. G. Tsikalakis and N. D. Hatziargyriou, "Centralized control for optimizing microgrids operation," *IEEE Trans. Energy Conversion*, vol. 23, no. 1, Mar. 2008.

[9] J. A. P. Lopes, C. L. Moreira, and A. G. Madureria, "Defining control strategies for microgrids islanded operation," *IEEE Trans. Power Syst.*, vol. 12, no. 2, May 2006.

[10] S. Ahn, J. Park, I. Chung, S. Moon, S. Kang, and S. Nam, "Power-sharing method of multiple distributed generators considering control modes and configurations of a microgrid," *IEEE Trans. Power Delivery*, vol. 25, no. 3, Jul. 2010.

[11] F. Katiraei and M. R. Iravani, "Power management strategies for a microgrid with multiple distributed generation units," *IEEE Trans. Power Syst.*, vol. 21, no. 4, Nov. 2006.

[12] P. Jahangiri and M. Fotuhi-Firuzabad, "Reliability assessment of distributed system with distributed generation," in *Proc. IEEE 2nd Conference on Power and Energy, PECon*, Dec. 2008, pp. 1551–1556.

[13] M. Fotuhi-Firuzabad and A. Rajabi-Ghahnavie, "An analytical method to consider DG impacts on distribution system reliability," in *Proc. IEEE Transmission and Distribution Conference and Exhibition*, Aug. 2005, pp. 1–6.

[14] S. Kennedy and M. Marden, "Reliability of islanded microgrids with stochastic generation and prioritized load," in *IEEE Powertech*, Bucharest, Jun. 2009.

[15] I. Bae and J. Kim, "Reliability evaluation of customers in a microgrid," *IEEE Trans. Power Syst.*, vol. 23, no. 3, Aug. 2008.

[16] R. Billinton and R. Allan, *Reliability Evaluation of Power Systems*, 2nd ed. London: Plenum Publishing Corporation, 1996, New York.

[17] L. Wu, M. Shahidehpour, and T. Li, "Stochastic security-constrained unit commitment," *IEEE Trans. Power Syst.*, vol. 22, no. 2, pp. 800–811, May 2007.

[18] L. Wu, M. Shahidehpour, and Z. Li, "GENCO's risk-constrained hydrothermal scheduling," *IEEE Trans. Power Syst.*, vol. 23, no. 4, pp. 1847–1858, Nov. 2008.

[19] P. Glasserman, *Monte Carlo Method in Financial Engineering*. New York: Springer, 2003.

[20] C. E. Lin, Y. S. Shiao, C. L. Huang, and P. S. Sung, "A real and reactive power control approach for battery energy storage system," *IEEE Trans. Power Syst.*, vol. 7, no. 3, pp. 1132–1140, 1992.

[21] M. Shahidehpour and Y. Fu, "Benders decomposition: Applying Benders decomposition to power systems," *IEEE Power and Energy Magazine*, vol. 3, no. 2, pp. 20–21, March 2005.

[22] Y. Fu, M. Shahidehpour, and Z. Li, "Security-constrained unit commitment with ac constraints," *IEEE Trans. Power Systems*, vol. 20, no. 3, pp. 1538–1550, Aug. 2005.

[23] Y. Fu, M. Shahidehpour, and Z. Li, "AC contingency dispatch based on security-constrained unit commitment," *IEEE Trans. Power Systems*, vol. 21, no. 2, pp. 897–908, May 2006.

[24] A. Flueck and Z. Li, "Destination: Perfection," *IEEE Power and Energy Magazine*, vol. 6, no. 6, pp. 36–47, Nov. 2008.

[25] IIT Perfect Power Prototype Final Report Endurant Energy, Oct. 2007 [Online]. Available: http://www.galvinpower.org

[26] ComEd Residential Real-Time Price (RRTP) of Electricity in Chicago [Online]. Available: http://www.thewattspot.com/

[27] J. Dupačová, N. Gröwe-Kuska, and W. Römisch, "Scenario reduction in stochastic programming: An approach using probability metrics," *Math. Program*, ser. A 95, pp. 493–511, 2003.

[28] GAMS/SCENRED Documentation [Online]. Available: http://www.gams.com/docs/document.htm

Mohammad E. Khodayar (S'09) received his MS degree in electrical engineering from Sharif University of Technology, Tehran, Iran in 2006. He is a Ph.D student in electrical engineering at Illinois Institute of Technology. His research interests include power system operation and planning.

Masoud Barati (S'09) is a Ph.D. student in the Electrical and Computer Engineering Department at the Illinois Institute of Technology, Chicago.

His research interests include operation and economics in smart grid.

Mohammad Shahidehpour (F'01) is the Bodine Professor and Director of the Robert W. Galvin Center for Electricity Innovation at Illinois Institute of Technology, Chicago. He is an Honorary Professor in the King Abdulaziz University in Saudi Arabia, North China Electric Power University, and Sharif University of Technology in Iran.